Geophysical Research Letters

Supporting Information for

Variability in Io's Volcanism on Timescales of Periodic Orbital Changes

Authors: Katherine de Kleer[1], Francis Nimmo[2], Edwin Kite[3]

[1]California Institute of Technology.

[2]The University of California, Santa Cruz.

[3]The University of Chicago.

Contents of this file

Text S1 to S2
Figures S1 to S4
Data Set S1

Introduction

The supporting information contains one section describing the geophysical model for Io's poroelastic tidal response (Text S1; Figures S1, S2) and a second section describing the relationship between the tidal forcing and the poroelastic response (Text S2; Figures S3, S4). Data Set S1 contains the compiled flux densities of Loki Patera from adaptive optics observations in 2001-2018.

Text S1: Io's poroelastic tidal response

Figure S1 is a sketch of the situation we envisage. A magma filled volcanic conduit is treated as a pipe of radius r with its base embedded in a partially-molten zone. Tidal stresses will deform this zone and flush melt in and out of the conduit, in a similar manner to water being squeezed out of a sponge. This flow will cause the level of magma in the conduit to oscillate with an amplitude h; this oscillation is presumed to result in the observed variations at the surface. The key point is that the amplitude increases as the forcing period increases, as explored in more detail below.

This situation is analogous to the well-studied case of tidally-driven water-well fluctuations on Earth [*Hsieh et al.* 1987; *Doan and Brodsky* 2006]. The response amplitude h of the fluid in the conduit can be written

$$h = \frac{h_0}{1+\frac{zK_0(z)}{2SK_1(z)}} \quad (1)$$

where h_0 is the asymptotic amplitude (given below), K_0 and K_1 are modified Bessel functions and z is a dimensionless number

$$z = r\sqrt{i\omega S/T} \quad (2)$$

where r is the conduit radius, ω is the angular forcing frequency and T and S are poroelastic characteristics of the partially-molten zone [*Wang* 2000]. T is the transmissivity (m^2s^{-1}), which mainly influences the response amplitude h, and S is the storativity (dimensionless) which controls the phase. The parameter z compares the forcing timescale with the characteristic timescale for the fluid to move a distance r. If z is small the fluid moves rapidly compared to the forcing, the amplitude saturates to h_0 and the response is in phase with the forcing. Larger values of z (e.g. shorter period forcing) result in smaller amplitudes and larger phase lags. Of course, all these parameters are poorly constrained for our situation of interest.

Assuming that the rigidity of the matrix (rock) dominates, the asymptotic amplitude h_0 is given by

$$h_0 \approx \frac{K_f}{\emptyset\rho g}\varepsilon$$

where K_f is the fluid bulk modulus, ρ is the fluid density, g the acceleration due to gravity, ϕ the porosity (melt fraction) and ε the tidal strain. In the case of a rigid matrix, the imposed strain is accommodated by the fluid, resulting in the $1/\phi$ dependence. For the same imposed strain, a higher K_f results in a higher fluid pressure. Basaltic melts have a bulk modulus of about 10-20 GPa [*Stolper et al.* 1981] so for a strain of 10^{-5} and 20% melt fraction the asymptotic amplitude is about 200 m. On Io the tidal strain is roughly $2\text{x}10^{-5}$ h_2, where h_2 is the Love number *(e.g. Bierson and Nimmo* [2016]*)*.

Again assuming that the matrix rigidity dominates, the transmissivity T and storativity S are given by *(e.g. Wang* [2000]*)*

$$T = \frac{k\rho gb}{\mu}$$

and

$$S = \frac{\rho gb}{K}$$

where k is the permeability, μ is the fluid viscosity and K the matrix bulk modulus. The quantity S/T in equation (2) is thus given by μ/kK, showing that the motion of the fluid depends on the characteristics of both the fluid itself (μ) and the matrix (k,K). Lower

viscosities, higher permeabilities and higher bulk moduli result in more rapid fluid transport. So we can rewrite equation (2) as

$$z \approx r\sqrt{i\omega\mu/kK} \qquad (3)$$

Of these quantities, probably the most uncertain is the permeability k (though the bulk modulus may be influenced to an unknown extent by the presence of exsolved gases). It is typically assumed that $k=Cd^n\phi^m$ with n=2, d is the grain size and C=0.01 when m=3 [*McKenzie* 1989]. So for 20% melt the permeability might be of order 10^{-10} m^2, but this is very uncertain. Assuming this permeability, taking r=100 m, μ=100 Pa s for basaltic magma and K=30 GPa we find $z\sim10^{-1}$ at 500-day periods, while at the diurnal period $z\sim4$. So one would expect h to approach the saturation amplitude at 500 days but not on diurnal timescales. For b=3 km with a density of 2.9 g/cc and g=1.8 ms^{-2}, S=5x10^{-4}.

Figure S2a shows the normalized amplitude (h/h_0) as a function of forcing period using equation (1). The main result is that, over a wide range of permeabilities, the response amplitude at diurnal periods is smaller by a factor of ~100 than at 500-day periods. If the permeability is less than 10^{-8} m^2 the response amplitude at 500 days will be less than the saturation value h_0. The Love number at diurnal periods is a factor of ~2 lower than at 500-day periods. So the normalized amplitude would be a factor of ~200 lower at diurnal periods than 500-day periods, other things being equal.

Figure S2b shows the phase lag between the tidal forcing and the conduit response. For the confined partial melt region (aquifer) that we assume the response at short periods is expected to lag the forcing (negative values); at longer periods the predicted phase lag depends strongly on the permeability assumed. An unconfined aquifer would show a positive phase shift.

Text S2: Linking orbital variations to poroelastic response

Our approach is predicated on the idea that variations in orbital parameters are driving the variable activity at Loki Patera. To investigate these periodic strains and phase lags we adopt the procedure laid out in Nimmo et al. (2014). In order to build intuition, we first do a similar calculation for the south pole of Enceladus and consider diurnal tides before addressing longer-period effects.

Stress variations

Figure S1a shows how the diurnal east-west ($\sigma_{\phi\phi}$), north-south ($\sigma_{\theta\theta}$) and shear ($\sigma_{\theta\phi}$) stresses vary with mean anomaly for a region at 315° W, 80° S on Enceladus. With one exception, parameters were selected to allow direct comparison with Fig 3a of Smith-Konter and Pappalardo (2008), hereafter SKP. The exception is that SKP take the Love numbers to be h_2=0.2 and l_2=0.04, whereas in the Nimmo et al. (2014) approach h_2 is constrained to be $4l_2$, so we take h_2=0.2 and l_2=0.05 (see discussion in Nimmo et al.

2014). This difference explains the small discrepancies between this figure and Fig 3a of SKP, especially in the shear stresses.

Figure S3b plots the variation in principal stresses, σ_1,σ_2 derived from $\sigma_{\phi\phi}$, $\sigma_{\theta\theta}$ and $\sigma_{\theta\phi}$ using equation 2-51 of Turcotte & Schubert (2002). Here we have normalized these stresses by the maximum positive value. We also plot the normalized quantity $\sigma_1+\sigma_2$, which will be directly proportional to the areal strain. This quantity reaches its maximum tensile (positive) value at apoapse, and its most compressional (negative) value at periapse, in agreement with SKP. The physical reason is that the tidal/rotational flattening is largest at periapse, resulting in polar compression, and smallest at apoapse.

Although the radial stresses are zero only at the surface, at sufficiently shallow depths $\sigma_1+\sigma_2$ will also be directly proportional to the volumetric strain, as long as the material is compressible. It is the volumetric strain which controls the permeable flow in the aquifer (Text S1 above).

Figure S4a is the same as Figure S3a except now using parameters appropriate for Io and evaluated at the location of Loki Patera (13°N, 309°W). The stresses are much larger, because of Io's proximity to massive Jupiter. Figure S4b plots the same quantities as Figure S3b but again for Loki Patera. This time the volumetric strain is tensile in the first half of the orbit (mean anomaly 0-180°) and compressional in the second half. A feature on the tidal axis would experience maximum tensional strain at periapse (where the tidal bulge is largest); Loki Patera's location off the tidal axis pushes the tensile stress maximum to ~90° later in the orbit. Equivalently, the expected peak compressional strain leads the minimum distance to Jupiter by ~90°.

Phase Shift

In considering the predicted phase shift between the orbital forcing and the observed response at Loki Patera, there are several effects to consider. There will be a phase offset between periapse passage and peak volumetric stress (1). Then there will be a phase lag between peak volumetric stress and the response of the fluid in the conduit (2). And, last, there may be a phase lag between the conduit fluid response and surface changes (3).

1. Diurnal variations in the distance to Jupiter result in diurnal variations in Io's shape, relative to its mean ellipsoidal shape. It is these variations that generate stresses (Figure S4). Similarly, longer-period variations in the distance to Jupiter result in variations in the mean ellipsoidal shape, which will again give rise to stresses. Because the long- and short-period shape variations have the same spatial pattern, the phase lag relative to the minimum distance to Jupiter will be the same. Thus, we expect the long-period peak compressional stress at Loki Patera to lead periods of closest approach to Jupiter (highest eccentricity) in the same way as the diurnal stresses (Figure S4b); that is, by ~90°.

2. Volumetric compression will cause the fluid in the conduit to rise, and vice versa. Depending on the material properties and forcing period, the response of the aquifer to

the strain is expected to lag the strain by 0° to 70° (Figure S2b). At the long periods of interest, the phase lag is ~70° over a wide range of permeabilities.

3. The poroelastic model focuses on variations in conduit height. It is assumed that these variations result in a surface expression (brightness changes). There may be some additional time delay between the conduit height variations and the surface change, but this effect is probably small: a time delay of 10 days (implying a vertical propagation rate of order 1 cm/s) would only change the phase by 8°).

The peak compressional strain leads periapse passage by ~90°. The aquifer response is expected to lag this peak compressional strain by ~70°. Thus, the overall prediction is that the surface response will lead periapse passage by ~20°, with any additional time delays reducing this amount. At even longer forcing periods, the aquifer response lag will be smaller and so the overall phase advance will be larger.

We therefore expect the long-period peak fluid height, and by presumption the peak activity, to lead the occurrence of smallest periapse (and highest eccentricity) by ~20°, minus any time delay effects. The clustering of observed activity around 0° phase lag with respect to eccentricity for the long-period forcing is thus in rough agreement with our predictions.

In contrast, an unconfined aquifer would lead the peak compressional strain by ~70° so the overall result would be a response almost out of phase with periapse passage. This result is not supported by the observations.

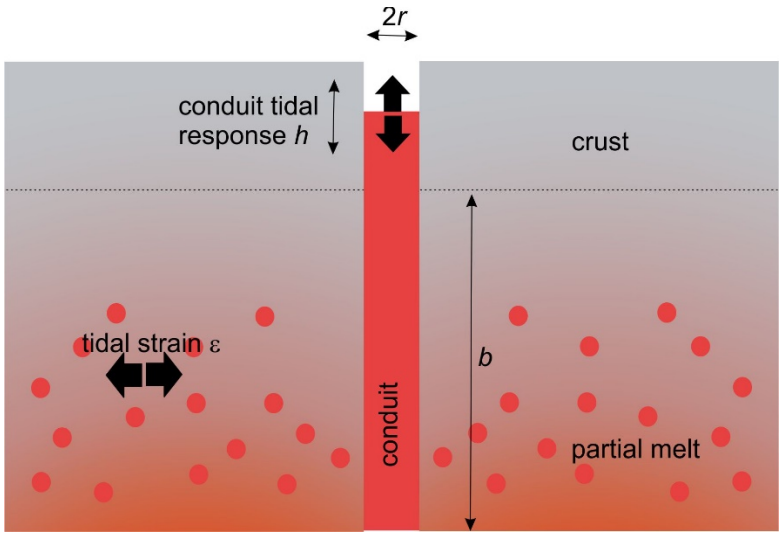

Figure S1. Definition sketch. Tidal strains flush melt in and out of the volcanic conduit, causing the magma level to rise and fall.

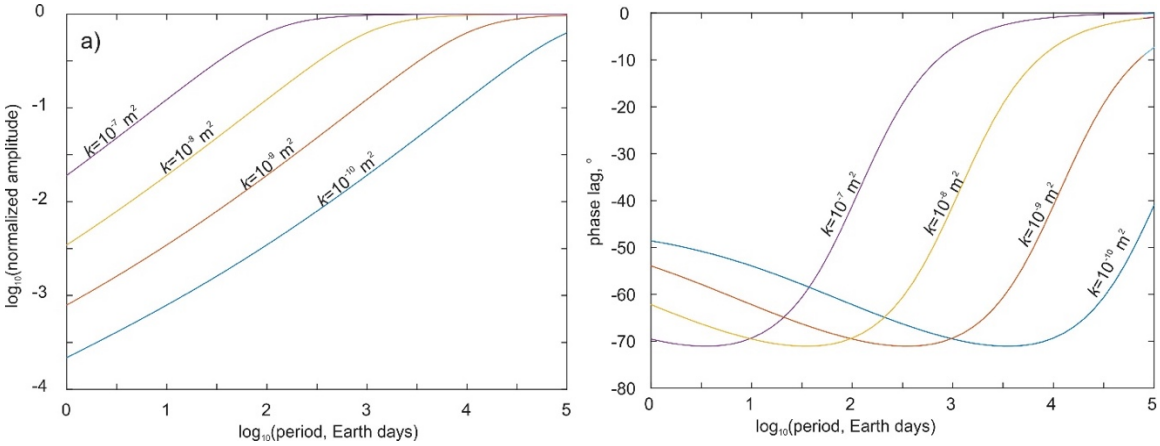

Figure S2. Tidal response. Normalized amplitude (h/h_0) and phase of the conduit tidal response as a function of the forcing period, calculated using equations (1) and (3) with different assumed values of permeability k. Here r=100 m, K_f=20 GPa, K=30 GPa, μ=100 Pa s.

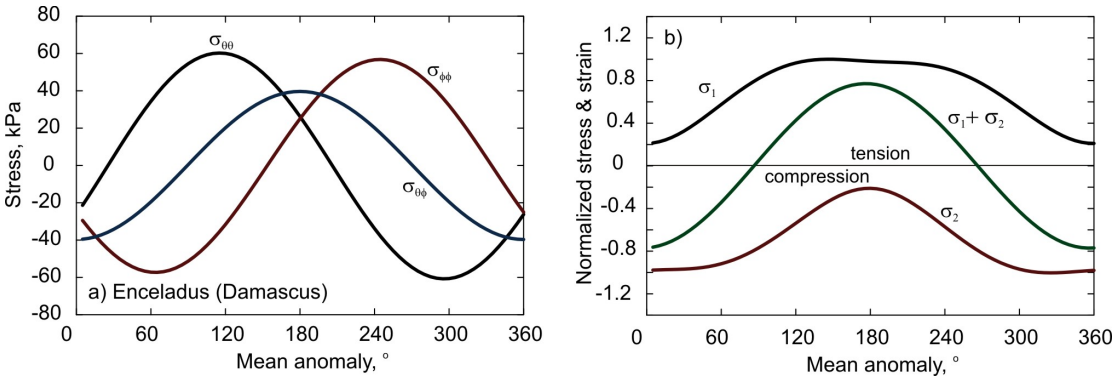

Figure S3. a) Variation in normal and shear stresses due to diurnal tides on Enceladus at 315°W, 80°S**.** b) Normalized principal stresses σ_1 and σ_2 (see text) at same location. The quantity $\sigma_1+\sigma_2$ is proportional to the volumetric strain. Parameters assumed: radius 252 km, g=0.113 ms^{-2}, semi-major axis 252,000 km, eccentricity 0.0047, primary mass 5.68x10^{26} kg, h_2=0.2, l_2=0.05, Lame parameters μ=3.5 GPa, λ=6.8 GPa.

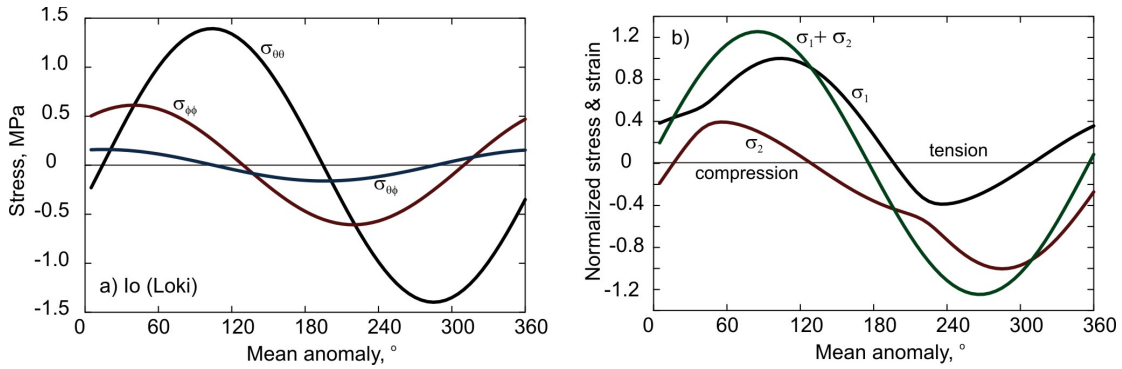

Figure S4 a). As for Figure S3a, but with Io parameters and evaluated at Loki Patera (13°N, 309°W). b) As for Figure S3b, but with Io parameters: radius 1820 km, g=1.796 ms^{-2}, semi-major axis 422,000 km, eccentricity 0.0041, primary mass 1.9x10^{27} kg, h_2=1.5, l_2=0.375, Lame parameters μ=30 GPa, λ=60 GPa.

Data Set S1

Flux densities of Loki Patera from adaptive optics observations in 2001-2018, compiled from *de Kleer and de Pater* [2016]; *de Pater et al.* [2017]; and *de Kleer et al., in review.*